Extended Abstract of the Doctoral Thesis "A Dual Projection Imaging System To Characterize Crystallization Processes: Design and Applications"

Dr. Ashwin Kumar RAJAGOPALAN, ETH Zurich

Summary

Crystallization as a separation and purification process has been applied widely in fine chemicals, pharmaceuticals and food industries. It typically involves a number of fundamental phenomena – often poorly understood – like nucleation, growth, dissolution, breakage, to name a few. The lack of reliable monitoring and characterization tools inhibits attaining deeper insights into the mechanisms involved, which thereof affects the robust and optimal operation of these crystallization processes. The work presented in the doctoral thesis titled *"A Dual Projection Imaging System To Characterize Crystallization Processes: Design and Applications"*[1] led to improvements in the state-of-the-art imaging techniques for size and shape characterization of the solid phase in batch solution crystallization processes. These improvements led to several interesting and previously unexplored applications within the context of batch crystallization. Few of the key accomplishments of this doctoral thesis are

- enhancements to the hardware of a stereoscopic imaging device and to the imaging analysis routines to classify crystals observed by the imaging device into five different shape classes and to obtain a three-dimensional reconstruction of these crystals *(Chapter Two)*.
- assessing the reliability of commercial spectroscopic techniques to estimate solute concentration in batch crystallization processes and proposing a new approach based on volumetric reconstruction of crystals observed by the stereoscopic imaging device, to estimate the solute concentration *(Chapter Three)*.
- transformation of needle-like crystals to more equant crystals in a multistage cyclic process consisting of wet milling, dissolution, and growth stages, exploiting the online monitoring capabilities of the imaging device and simple feedback control laws for the individual stages *(Chapters Four through Six)*.

The results presented in the thesis reinforce the potential and the competence of imaging tools to tackle a wide array of challenges faced by the crystallization community. Irrespective of the promising outcome, their potential pitfalls are definitely not overlooked and plausible proposals to overcome these are discussed diligently to assist future research.

The following sections summarizes the five chapters that appear in the doctoral thesis. Each of these sections addresses the why and the how of the work presented in that given chapter along with the key results. This is followed by a small note on the relevance and impact of the doctoral thesis.

Chapter Two: Characterization of Particulate Populations in Suspension[2]

In crystallization processes, the particle size and shape of the final product obtained at the end of the crystallization step is of key importance as it influences the downstream processing operations.[3,4] Crystals exhibit different shapes depending on the crystal habit, and an accurate characterization of shape is critical in the design and control of such processes. Often, commercially available crystallization process characterization tools condense shape related information of crystals into a single characteristic length.[5] Commercially available sizing tools that rely on the assumption of a single characteristic length, such as focused beam reflectance measurement (FBRM), laser diffraction, Coulter counter, as well as monoscopic imaging tools, are prone to errors and misleading effects for nonspherical particles.[6] Multiprojection imaging systems,[7–11] have the ability to tackle shape-related issues rather satisfactorily, thus reducing the ill effects encountered by commercial sizing tools for nonspherical particles. The successful implementation of a dual projection imaging device using a stereoscopic camera setup with a sapphire glass based flow channel with an automated image analysis routine was already demonstrated.[11] However it was evident that the device would benefit from improvements to the hardware construction and to the image analysis routine.

To this aim, a state-of-the-art, compact optomechanical setup coupled with an image analysis routine to measure multidimensional particle size and shape distributions (nD PSSDs) for crystallization processes was conceived. The details of the design is presented in this chapter. The optomechanical setup referred to as the dual imaging system for crystallization observation (DISCO), shown in Figure 1, consists of two monochrome cameras with telecentric optics in an orthogonal configuration. Two high-power, telecentric LED illuminators, which emit collimated rays parallel to the optical axis produce high contrast silhouettes of parti-

cles passing through a single piece quartz square flow channel. The suspension is pumped from the crystallizer through the flow channel using a peristaltic pump. A high-speed image capture mode (up to a theoretical maximum frame rate of 75 Hz), capable of monitoring processes with fast kinetics, is also introduced.
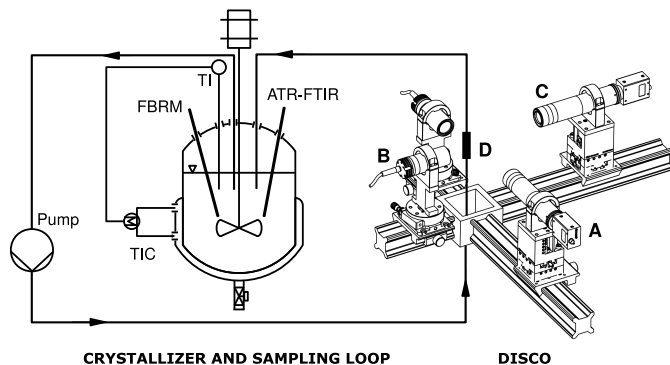

Figure 1: Schematic of the dual imaging system for crystallization observation (DISCO). The suspension flowing from the crystallizer through the flow channel (D) is backlight illuminated using two telecentric illuminators (B). The suspension is imaged using two digital cameras (A) with telecentric optics (C). The camera, lens and the illuminator system are mounted orthogonally on an optical rail construction.

A novel image processing pipeline to process the raw images from the cameras is presented. The pipeline consists of a stereoscopic camera calibration model, adaptive background subtraction, particle contour matching, and 3D reconstruction of the segmented crystals. The reconstructed crystals are subjected to a supervised shape classification strategy, which categorizes each detected crystal into spheres, needles, quasi-equant particles, platelets, and non-convex particles. This multistep image processing approach is visualized in Figure 2.

The DISCO is then subjected to a thorough experimental campaign, to validate size measurements, to characterize steady-state, and to confirm repeatability of measurements to affirm and to assess the non-invasive nature of the setup on the measurement. An experiment aimed at evaluating the enhancement in the proposed image analysis pipeline performance, more specifically the automatic shape classification, is presented. These experiments help highlight the ability of the DISCO to track shape changes with a time resolution an order of magnitude higher when compared to the previous iteration of the dual projection imaging device. Finally, the positive outcome from the experiment concerning the dissolution – which often proceeds in time scales in the order of a few minutes – of a needle-like is the first step toward quantitatively monitoring, characterizing, and modeling a dissolution process using a stereoscopic imaging setup. This has been put to use to estimate the dissolution kinetics of a needle-like compound.[12,13]

It is worth acknowledging the fact that the long sequence of image processing steps going from the two raw images to the final size and shape distributions introduces several uncertainties. The camera-lens system introduces an optical error, while the assumption of a generic particle model introduces a geometrical error. Alas, the quantification of such errors is a nontrivial task, which is beyond the scope of this chapter. The 3D reconstruction method presented here is merely an upper bound approximation of the three-dimensional particle shape as long as only two projections are available. There is certainly no doubt that the output from the shape classification model is a qualitative result, which is not necessarily linked to physical quantities. It goes without saying that considering the mentioned limitations, the output from the measurements should be analyzed with care, to avoid over-interpretation. To conclude, the improvements will have a profound impact in making size and shape feedback control of a process possible, which will become evident in the subsequent sections.

Chapter Three: Alternative Approach to Solute Concentration Estimation[14]

In order to accurately describe crystallization phenomena and to further control the process, the ability to obtain robust information of the solid and liquid phase, preferably online, is a prerequisite. Within the context of this work, the solid phase can be monitored and characterized using the DISCO presented in Chapter Two. The liquid phase is usually monitored and characterized using spectroscopic or chromatographic techniques, such as attenuated total reflectance Fourier transform infrared spectroscopy, attenuated total reflectance ultraviolet/visible spectroscopy,[15] Raman spectroscopy,[15,16] high-performance liquid chromatography, and ultra-performance liquid chromatography.[17] In some batch crystallization processes, unfavorable experimental conditions, the time required to obtain the concentration estimate, or a combination of these factors may prohibit the use of commercially available techniques to accurately observe the evolution of the solute concentration. Due to the inherent challenges posed by conventional and commercially available techniques to estimate the solute concentration for the aforementioned systems, an alternative approach to estimate solute concentration in seeded batch crystallization processes is presented in this chapter.

In a seeded batch crystallization process where no reactions occur, the presence of solid particles and their change over time inherently contains information regarding the liquid phase through the mass conservation constraint, i.e., an increase in the mass of the crystals is reflected as a decrease in the solute concentration, and vice-versa. This basic principle can be exploited by means of multiprojection imaging
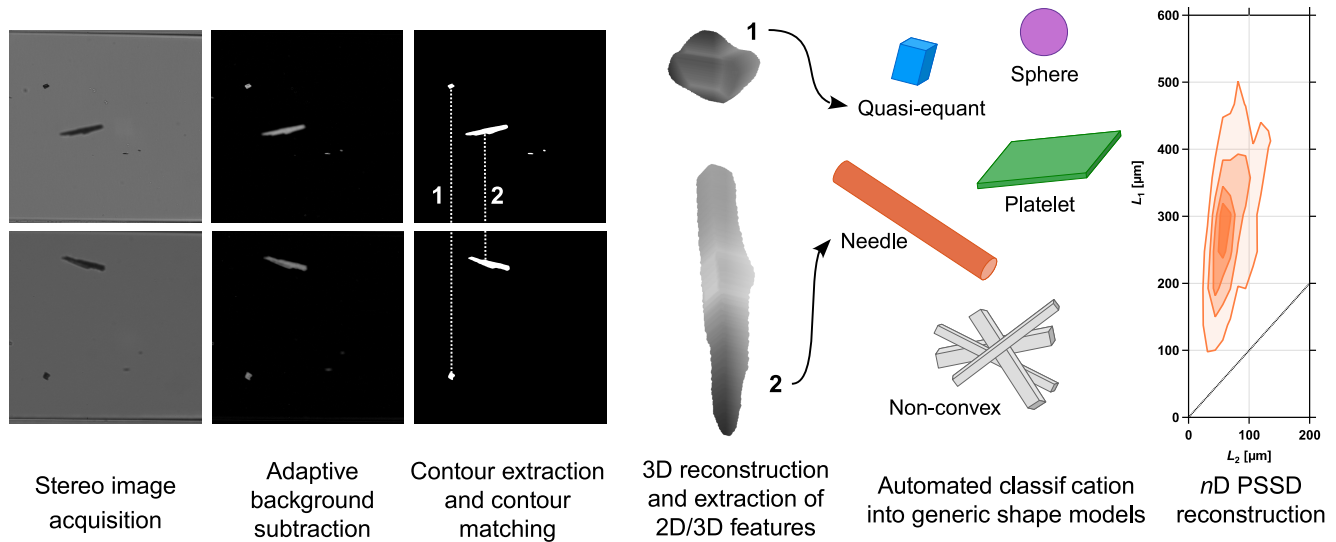
Figure 2: Illustration of the multistep image processing approach. This includes the adaptive background subtraction, a contour matching algorithm, 3D shape reconstruction, and the automated shape classification of reconstructed particles. The result of this procedure is an nD PSSD for each generic shape model.

devices that provide time-resolved measurements of the volume of the particles. The DISCO (see Chapter Two)[2] provide an estimate of the visual hull[18] of the observed particles. The volume of a specific visual hull can be seen as an approximation to the volume of the corresponding particle. This quantity is obtained by estimating and summing up the visual hull volumes of all the particles imaged within a short period of time. Thus, the change in the solute concentration based on the observed change in the total visual hull volume is inferred from the material balance given by

$$\hat{c}(t) = c_0 - \rho_c \big(\phi_v \hat{V}(t) - V_{\text{seed}} \big) \qquad (1)$$

where $\hat{c}$ and c_0 are the estimated solute concentration at time t and the known initial solute concentration, respectively, both on a per mass of solvent basis. ρ_c is the particle density, ϕ_v is a scaling factor, $\hat{V}$ is the total visual hull volume observed at time t, and V_{seed} is the volume of seeds added per mass of solvent. Note that since the measurement approach of DISCO is based on sampling particles from a crystallizer, the scaling factor ϕ_v has to be introduced to account for the difference in the volume of particles observed by the device $\hat{V}$ in the time interval between t and $t + \Delta t$ and the total volume of particles in the crystallizer.

A series of seeded batch experiments are carried out to obtain the solubility curves for two different compounds using the proposed method. Small amounts of the compound of interest are suspended in their respective saturated solutions, where these amounts are chosen so as there was only a small number of overlapping particles in the images taken by the DISCO. The suspensions are subjected to predefined heating ramps that drive them to slightly undersaturated conditions that should lead to the dissolution of solids

and an associated change in the solute concentration. Based on the experimental data obtained, Equation 1 is applied to estimate the evolution of the solute concentration over time for each experiment. Independently measured solubility curves obtained using ATR-FTIR spectroscopy reported in the literature[19,20] is used for comparison with the proposed method. Even though the method is approximate in nature, the solute concentration estimates obtained by observing the solid phase is promising, as the solubility measurements obtained in this study, for two different compounds exhibiting different seed characteristics in terms of particle shape,
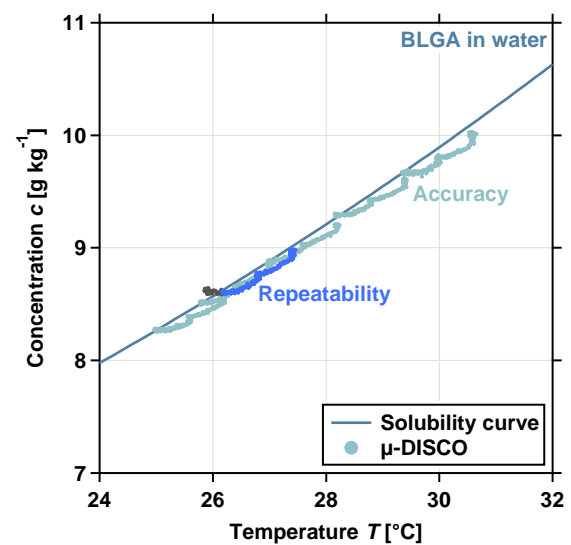

Figure 3: Solubility curve of BLGA in water reported in the literature[19] (solid blue line) and measured using the DISCO (solid markers). The light blue solid markers stays close to the literature solubility curve highlighting the accuracy of the proposed method. The dark blue solid markers overlaps over the light blue solid markers highlighting the repeatability of the measurement.

show good agreement with literature data (for instance see Figure 3 for β L-glutamic acid (BLGA)).

By performing additional measurements aimed at obtaining the solubility curves using ATR-FTIR and the DISCO, it is shown that the concentration estimates of both techniques are in good agreement with the literature data. However, a higher noise level in the concentration estimate obtained from ATR-FTIR is observed when compared with the one obtained from the DISCO over the whole temperature range explored highlighting the inherent limitations of the spectroscopic technique for the given system. Based on a simple error propagation on Equation 1, it is shown that the errors in the concentration estimate arising from the uncertainties in the visual hull volume are small in magnitude (see the doctoral thesis [1]). But note that obtaining a solubility curve using IR spectroscopy enables exploring larger ranges of temperature and enables distinguishing different species in solution, which is not possible with the proposed approach. To conclude, the proposed method can be useful in situations where employing commercially available standard solute concentration monitoring tools is challenging. Additionally, in the development phase of fine chemical production processes, both the solid and the liquid phase could be characterized using the same device (in this case the DISCO).

Chapter Four: Manipulation of Size and Shape in Cooling Crystallization[21]

Feedback control approaches have been proposed to control primarily the size and more recently the shape of particles in a population during crystallization processes.[22–24] It is well known that the particle size and shape influence downstream processing operations. Alas, experimental studies applying feedback control based on particle size and shape measurements are scarce in the literature,[25,26] as the required online monitoring devices are not yet widely available. The availability of an online monitoring tool (DISCO, for PSSD and solute concentration) and the the availability of a model-free path following control (PFC) scheme proposed previously[27] for a seeded, growth-dominated batch cooling crystallization processes facilitates the experimental validation of the proposed controller for a robust manipulation of crystal size and shape. The goal of this control strategy is to guide the evolution of the average size and shape of a seed population of needle-like crystals into a target region in the crystal size and shape space. The control strategy does not require any crystal growth rate models, but requires only the solubility data for the considered solute and solvent in the temperature range of interest.

The assumption behind controlling the evolution of the average dimensions is that the ratio of the rate of change of the two average dimensions $\frac{\mathrm{d}\bar{L}_1}{\mathrm{d}t}/\frac{\mathrm{d}\bar{L}_2}{\mathrm{d}t}$ is a monotonic function of the process temperature. This assumption is critical as it allows the crystal size and shape to be influenced by soleley changing the process temperature (hence the supersaturation), in the absence of other external actuators.[27] Note that the crystal size and shape space for a needle-like compound is spanned by the average length $\bar{L}_1$ and the average width $\bar{L}_2$ of the particles in these populations. Growing seed populations of compounds characterized by multiple average dimensions and subjected to constraints on temperature and supersaturation, where the monotonicity assumption in the temperature (or in the supersaturation) is satisified, exhibit an attainable region for crystal size and shape.[26,28] Subsequently, a population of seed crystals with measured average dimensions can be directed toward target average dimensions chosen to lie within this attainable region using the PFC strategy. The PFC is implemented as a proportional-integral (PI) controller which tries to keep the measured average dimensions of the PSSD in the crystal size and shape space close to a reference path that connects the measured average dimensions of the seed population and the target average dimensions. The perpendicular distance between the point with coordinates given by the measured average dimensions and the reference path $e(t)$ is computed at every point in time when a new measurement of these average dimensions becomes available. The distance $e(t)$ serves as the control error and is PI filtered to produce a feedback contribution $\Delta T_{\mathrm{fb}}(t)$ to the process temperature set point that is given as

$$\Delta T_{\mathrm{fb}}(t) = k_{\mathrm{p}}\Big(e(t) + \frac{1}{\tau_{\mathrm{I}}}\int_{t_0}^{t} e(s)\,\mathrm{d}s\Big) \qquad (2)$$

where k_{p} and τ_{I} are the PI tuning parameters and t_0 is the time at which the controller action is initiated. The feedback contribution obtained from Equation 2 is then added to a feedforward temperature set point $T_{\mathrm{ff}}(t)$ to obtain the process temperature set point

$$T_{\mathrm{set}}(t) = T_{\mathrm{ff}}(t) + \Delta T_{\mathrm{fb}}(t) \qquad (3)$$

After enforcing constraints on both the supersaturation and the temperature, this set point is sent to a low-level temperature controller in the thermostat.[27]

To select sensible target average particle dimensions for batches controlled by the PFC, it is beneficial to estimate the attainable region for crystal size and shape for a given seed population. After confirming the monotonicity assumption, it will be clear that the attainable region for a given seed population and for the chosen supersaturation limits is bounded by the two trajectories obtained with the supersaturation kept constant at its two extremal values. To this aim, con-
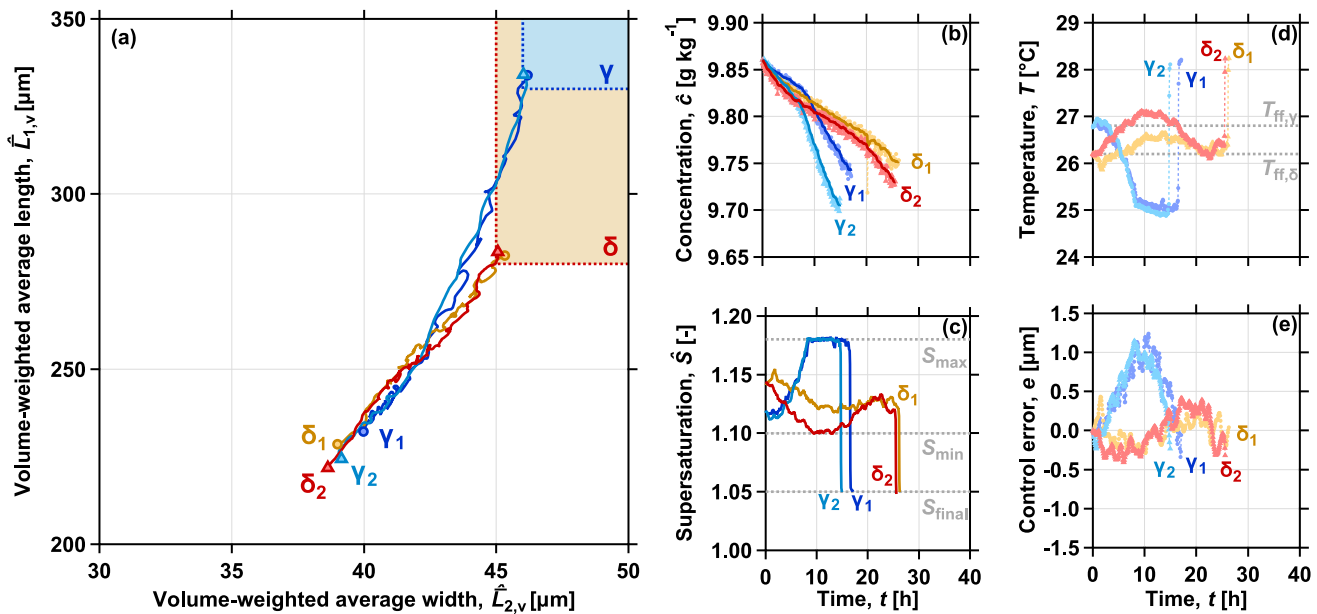
Figure 4: PFC experiments for the first batch of seeds. **(a)** Evolution of the low-pass filtered volume-weighted average dimensions in the crystal size and shape space for two different target dimensions $[\bar{L}_{1,\text{target}} \ \bar{L}_{2,\text{target}}]^{\text{T}}$, namely, $[330 \ 46]^{\text{T}}$ µm (γ) and $[280 \ 45]^{\text{T}}$ µm (δ). The subscripts denote the repetition of the PFC experiment performed for each target. **(b)** Evolution of the solute concentration. The solid markers represent the concentration estimate $\hat{c}$ and the solid lines represent the low-pass filtered concentration $\hat{c}_{\text{filt}}$. **(c)** Evolution of the supersaturation $\hat{S}$. **(d)** Evolution of the measured process temperature T. **(e)** Evolution of the control error e.

stant supersaturation controller (CSC) experiments are performed with two chosen batches of BLGA seed crystals at four constant supersaturation levels, all of them within the predefined supersaturation limits. The results of the CSC experiments also allow to select the correct sign of k_{p} in Equation 2 for subsequent PFC experiments. Based on the experiments using the two seed batches two observations stand out. First, as expected for the needle-like BLGA in water, the population grows preferentially along the L_1 direction. Second, a cone-like area is observed in the size and shape space, with the trajectory corresponding to experiment with the upper bound of the supersaturation limit as the upper boundary and that of experiment with the lower bound of the supersaturation limit as the lower boundary. Additionally, it can be said that the attainable region is narrow for both batches of seeds and can be attributed to how BLGA crystals grow in water within the ranges of operating conditions explored. Finally, concerning the monotonicity assumption and the general shape of the attainable region, the two batches behave similarly and thus, it is concluded from these experiments that the PFC strategy can be applied.

An experimental campaign aimed at growing different batches of BLGA crystals to reach different target dimensions within the attainable regions is carried out. For each of the two seed populations, two different target average dimensions are chosen in the crystal size and shape space spanned by the volume-weighted average length and width of the populations. The experiments are repeated to assess

if the control scheme is robust enough to guide the seed population toward the desired target dimensions repeatedly. For the first batch of seeds, a total of four closed-loop experiments with the PFC are performed. The experiments with the two different targets are henceforth distinguished by referring to them as γ and δ. Similar targets are also chosen for the second batch of seeds. The outcomes of these four experiments are illustrated in Figure 4. From Figure 4a, it can be seen that the controller manages to guide the population very close to the assigned target points for all the four experiments. The slopes of the paths taken in the crystal size and shape space for targets γ and δ appear to be similar. But given the narrow attainable region of BLGA in water, the differences in the product aspect ratio for the two targets γ (7.2) and δ (6.2) are quite significant. The supersaturation and temperature profiles, shown in Figure 4c and Figure 4d, respectively, and the batch times also indicate that the seed population evolved rather differently when approaching the two targets. The excellent performance of the controller to reach the desired target is exhibited by the following two observations. For target γ, the control error shown in Figure 4e is positive for the first few hours, which indicates that the measured average size and shape is below the reference path. The controller manages to compensate for the increasing control error by lowering the temperature, thereby gradually increasing the supersaturation from the initial value to the upper bound. Unlike for target γ, for target δ the measured average dimensions stays relatively close to the ref-

erence path, which can be seen from the evolution of the control error in Figure 4e. Since the control error is negative initially, the controller slows down the growth of the population by increasing the temperature and thereby reducing the supersaturation from the initial value to values close to the lower bound. Finally, the two repetitions with target γ and δ evolves qualitatively similarly in terms of the concentration, the supersaturation, the temperature, and the batch time. Also, similar behavior of the controller is observed with the other seed batch (see the doctoral thesis[1]).

To conclude, the benefits of the proposed combination of online monitoring and feedback control is clearly demonstrated: a considerable level of robustness with respect to unexpected disturbances is achieved, which increases the repeatability and thus the predictability of the outcome of consecutive batches in this growth-dominated batch cooling crystallization process.

Chapter Five: Modeling and Control of a Rotor-Stator Wet Mill[29]

Milling is a widely applied unit operation during the production of solid pharmaceuticals and fine chemicals. It has the potential to strongly modify the particle size and shape, either during or after a crystallization step, which can increase the efficiency of various downstream unit operations and improve important quality attributes of the final product. It has the potential to strongly modify the particle size and shape, either during or after a crystallization step, which can increase the efficiency of various downstream unit operations and improve important quality attributes of the final product. For instance, milling can enhance bioavailability, tablet content uniformity, and powder compactability.[30,31] Wet milling is often employed to produce narrow crystal size distributions without altering the crystallinity of the solids. Because of the importance of wet milling in the pharmaceutical industry, significant efforts have been directed towards studying and modeling the breakage processes of suspended crystals, using both *in situ* and *ex situ* wet mills.[31–39] Studies in the literature demonstrate a number of benefits from integrating wet milling with crystallization processes. Alas, in all these studies, the mills were operated at predefined rotor speeds, thereby missing the opportunity to exploit the potential of applying feedback control to dynamically alter the rotor speed. Furthermore, most of the employed models were one-dimensional and the quantitative monitoring tools utilized in the experimental studies provided a one-dimensional PSD. Thus, the evolution of the particle shape was often neglected.

In this chapter, model-based and model-free operating policies and feedback control strategies to manipulate the size and the shape of needle-like crystals using a wet mill as the physical actuator are presented. Initially, these schemes are intended for a pure breakage process, but with the option of integrating them within a cyclic size and shape modification process involving also growth and dissolution stages (see Chapter Six). The attainable region for the average particle dimensions when undergoing wet milling is derived from a multidimensional population balance model incorporating breakage kinetics developed for the needle-like compound BLGA. Utilizing the same model, a model-based operating policy is presented with the goal to drive batches of BLGA seed crystals to different target average lengths in the size and shape space. Furthermore, simpler model-free feedback control laws are introduced. They are applied experimentally to the two needle-like compounds BLGA and γ D-mannitol (GDM). The DISCO presented in Chapter Two is employed to obtain the required feedback of the particle size and shape evolution.

Two milling configurations (*Two Crystallizer* and *Recirculation*) that are widely used are studied in detail in this chapter to increase the understanding of wet milling stages operated during or after crystallization steps. The structure of the two multidimensional population balance models that describe the two milling configurations exhibit differences. In order to better understand the differences that might potentially arise from employing either of the two milling configurations, a simulation study followed by an experimental validation of the same was undertaken. Based on the observations made from both the simulations and the experiments, it is shown that the two milling configurations are identical under the considered operating conditions (see the doctoral thesis[1]).

A better understanding of the two milling configurations facilitates size and shape manipulation using model-based operating and model-free control strategies. To this aim, first lab-scale experiments are designed and performed using a model-based operating policy. For these experiments, two different batches of BLGA seeds are used to reach three different target average lengths $\bar{L}_{1,\text{target}}$ for each batch of seeds. It is shown that the model-based operating strategy is able to drive the seed population close to the three targets for one batch of seeds. While, for the other batch of seeds the multidimensional breakage model used in the operating policy underpredicts the rotor speeds required to reach the targets. These experiments highlight the need to include a feedback control action to compensate for shortcomings of the employed process models. However, in the case of wet milling, the feedback controllers have to act cautiously, since milling is an inherently irreversible process. Following this, two different feedback control strategies and a benchmark policy are tested experimentally and compared. The controller that shows superior performance is then applied

with the goal to reach the same target average lengths as the previous case. Two performance criteria are assessed for all the controllers: first, their ability to reach a given target average length $\bar{L}_{1,\text{target}}$; then, the required number of full suspension passes through the wet mill to do so. After a careful evaluation, the so called adaptive *A controller* is chosen to perform further closed-loop control experiments due to its ability to reach the target average length by making use of the knowledge gained from prior milling stages regarding the evolution of the average length. The *A controller* learns a simple process model online from past data in the spirit of adaptive control. Since, the evolution of $\hat{\bar{L}}_{1,\text{v}}$ shows similarities to an exponential decay when the rotor speed is kept constant across the milling stages, a discrete-time model is built on-the-fly using the PSSD measurements obtained by the DISCO. The discrete-time model exhibits several favorable properties like dynamic nature, automatic determination of model parameters using online measurements, and a simple formulation that captures the physical trends.

The *A controller* is then employed to perform closed-loop control experiments using the *recirculation* configuration. A total of six experiments, three each for two batches of BLGA, are performed with a goal to reach the same targets as in the case of the experiments using the model-based operating policy. The resulting evolution of the volume-weighted average length and width and the rotor speed θ for each full suspension pass through the wet mill are shown in Figure 5a-c for one batch of seeds. Two main observations can be made from these plots. First, it is clear that the controller manages to drive the population to the target average length $\bar{L}_{1,\text{target}}$. A second observation is that the different experiments show a different evolution of the rotor speeds through the milling stages and a different number of full suspension passes required to reach the respective target. To highlight the superior performance of the adaptive controller when compared to the model-based operating policy, the product PSSDs from the corresponding experiments are also compared. It is essential that the control strategies proposed in this chapter can be applied to any given compound that exhibits a needle-like morphology. The proposed *A controller* should be able to drive the average length of a seed population towards a target length independently of the compound. Hence, to check if this is indeed the case, closed-loop control experiments with GDM, also exhibiting needle-like morphology, are performed using the *A controller*. Based on the observed evolution of the average length it is shown that the controller is successful in achieving its goal.

To conclude, to introduce robustness and to eliminate the dependency on multidimensional breakage models, model-free control laws are proposed that exploit the online monitoring capabilities of the DISCO. The successful control of wet
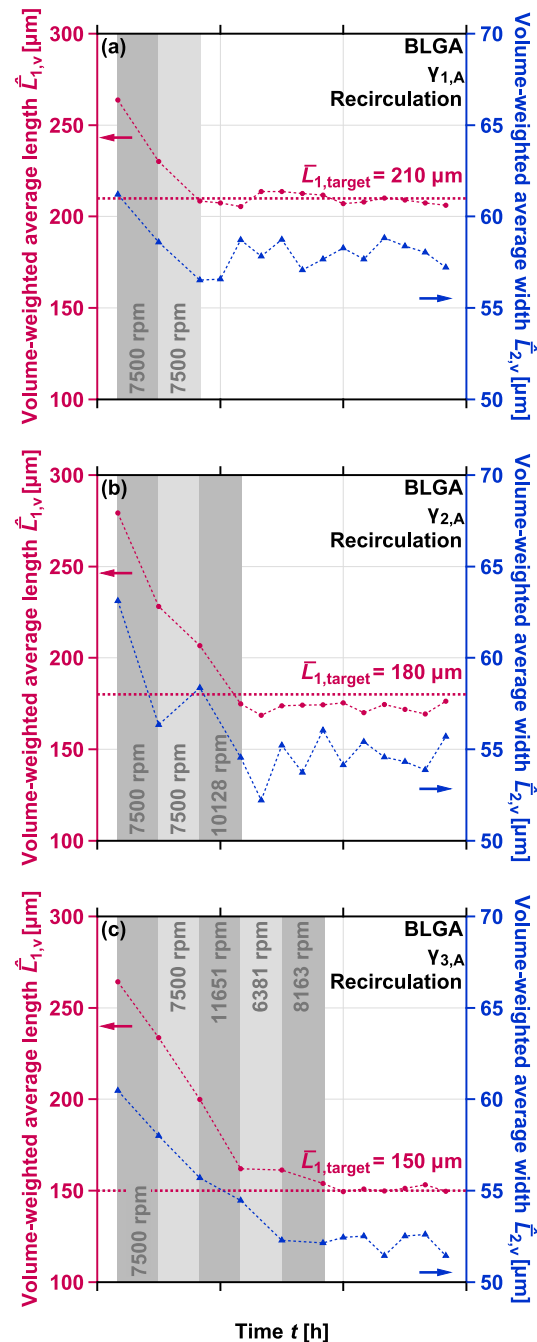

Figure 5: Time-resolved evolution of the measured volume-weighted average length $\hat{\bar{L}}_{1,\text{v}}$ and width $\hat{\bar{L}}_{2,\text{v}}$ for BLGA Seeds ε with target average lengths $\bar{L}_{1,\text{target}}$ **(a)** 210 μm ($\varepsilon_{1,A}$), **(b)** 180 μm ($\varepsilon_{2,A}$), and **(c)** 150 μm ($\varepsilon_{3,A}$) using the A controller. The shaded gray region in all the figures indicates the milling stage, and the corresponding rotor speed θ is reported alongside.

milling stages using model-free controllers is consistent with previous efforts to control growth-dominated batch crystallization processes in an entirely model-free fashion (see Chapter Four[21]), and represents a further step towards integrating different unit operations to robustly and effectively manipulate the size and shape of needle-like crystals (see Chapter Six[40]).

Chapter Six: Crystal Shape Engineering Using a Controlled Cyclic Process[40]

The purpose of this chapter is to present an experimental validation of a controlled and reproducible batch process that transforms needle-like seed crystals into more equant particles. While the process itself has been developed previously,[41,42] the focus of this chapter lies on two important novelties: first, the fully automated and controlled process operation in the absence of kinetic process models, and second, the robustness of the process control scheme with respect to achieving product PSSDs with consistent characteristics (in terms of average quantities) over consecutive batches. From a broader perspective, this chapter aims to integrate all the tools that developed in the previous chapters to monitor and to manipulate the size and shape of crystals in a batch crystallization process. To facilitate the manipulation of the particle shape, this process is operated in a cyclic fashion, where one cycle consists of three stages, namely, of a growth, a breakage, and a dissolution stage. These three stages serve different purposes: the growth stage (*g*) is a cooling crystallization step that generates yield and increases the size of the particles by crystallizing the solute from the liquid phase while avoiding observable nucleation; the breakage stage is a wet milling step (*m*) that reduces the particle aspect ratio (defined as the ratio of the particle length to the particle width) by mechanical action while leaving the yield unaffected; finally, the dissolution stage (*d*) is a heating step, during which many of the fines generated in the breakage stage are dissolved and the particle size and thus the aspect ratio can be reduced further depending on the operating conditions. The PSSD can be modified by altering the operating conditions of the individual stages, by varying the number of cycles, or by a combination thereof. Feedback controllers for each of the three stages are developed and validated individually (see Chapter Two and Chapter Four).[12,21,27,29] In this chapter, these controllers are combined to form a *controlled* multistage process. An important feature of the controllers for these individual stages is that they require only thermodynamic knowledge (i.e., solubility data) to operate the process, but no kinetic models. Since the proposed control laws operate the individual stages and not the whole cycle, a superordinate cycle logic is required that provides targets for the individual stage controllers on the basis of the overall process goals (see the doctoral thesis[1]). For many compounds exhibiting a needle-like morphology, often not much can be done to control the average particle width $\bar{L}_2$ during the single stages. Therefore, it is suggested here to specify only the intermediate and the final average lengths of the needle-like particles. A suitable superordinate cycle logic is then defined using only four parameters that specifies the reduction in the aspect ratio going from the seed population to the product population.

Two main goals are defined for the controlled process. First, it needs to be proven that the process indeed provides the desired reduction of the particle aspect ratio. Second, the generality of its application to a number of compounds is crucial as well, as it guarantees that the process is not tailor-made for a specific compound. A total of four studies are performed which would highlight the effect of the number of cycles on the product population, the insensitivity of the control strategy to the initial conditions, the repeatability of the control strategy to reach predefined targets, and the generality of the control strategy to be applied to a different compound. An experimental campaign is conducted using two different systems, namely, BLGA in water and GDM in a mixture of water and propan-2-ol. Apart from the fact that both BLGA and GDM crystals exhibit a needle-like morphology under the conditions explored in this chapter, other properties such as their thermodynamic (solubility) and kinetic (growth and dissolution rates) behavior are significantly different,[43] making them two suitable systems to test the effectiveness and the generality of the proposed controlled process. Note that the yield and the productivity are not considered to be goals of this process.

Three experiments were conducted with the system BLGA in water. In a preliminary phase, a given batch of BLGA seed crystals is grown to a given target average length by means of a growth stage at constant supersaturation. Subsequently, two cycles of the controlled multistage process are run to reduce the average particle aspect ratio of the particle populations obtained after this preliminary growth step. By varying the target average length of the preliminary growth step, the effect of differences in the initial conditions (seed population and initial solute concentration) is investigated. In each experiment, the aspect ratio reduction and in turn the final target size of the product population is achieved by defining the four parameters of the cycle logic. The low-pass filtered evolution of $\bar{L}_{1,\mathrm{v}}$ and $\bar{L}_{2,\mathrm{v}}$ plotted in Figure 6a shows that the controlled process operation enables the transformation of seed populations with different average dimensions (circular markers) into PSSDs with very similar average dimensions, either using one (downward pointing triangles) or two cycles (upward pointing triangles). Figure 6d illustrates that a reduction of the average particle aspect ratio over the two cycles is achieved, from an initial value of about 5 to 6 to a final value of about 3. Furthermore, Figure 6b,c indicates that also the broadness measure of the PSSDs along the L_1 direction decreases over the cycles, while that along the L_2 direction is barely affected. Clearly, this observation goes along with a reduction of the ratio of the broadness along the two dimensions ψ, as can be seen in Figure 6e. The duration of
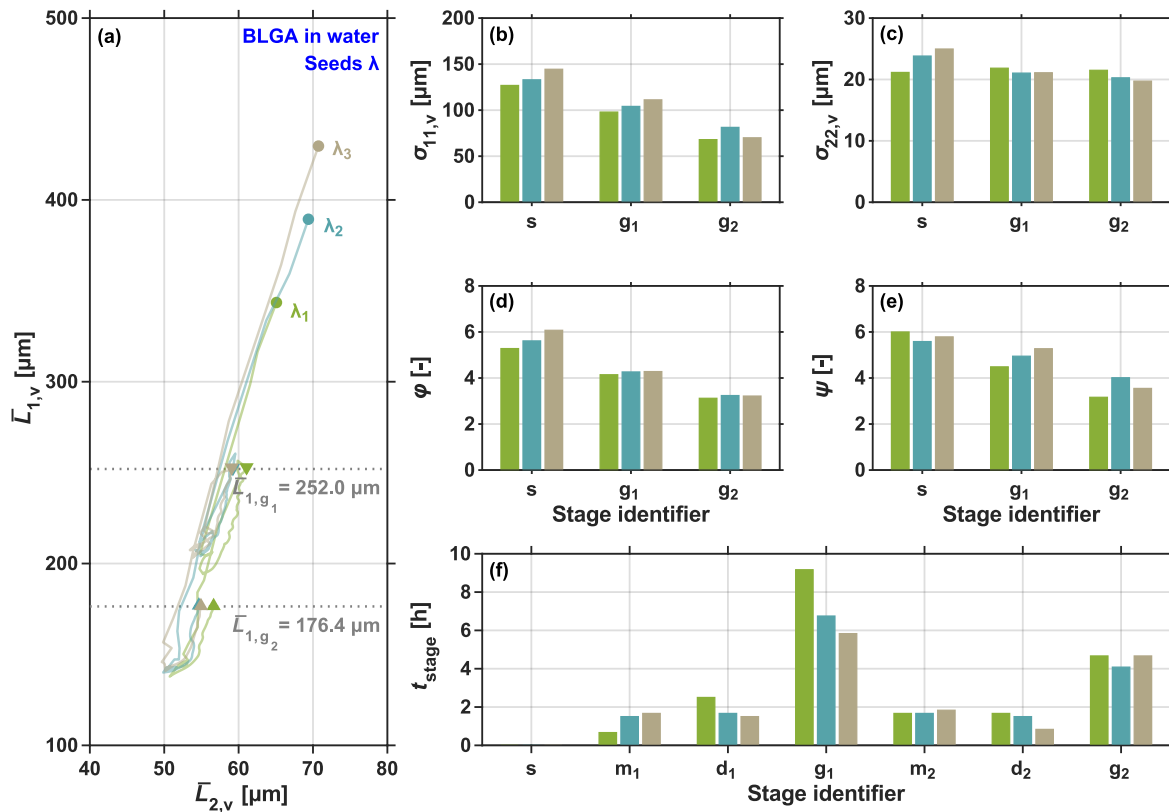
Figure 6: **(a)** Low-pass filtered evolution of the volume-weighted average length $\bar{L}_{1,\mathrm{v}}$ and width $\bar{L}_{2,\mathrm{v}}$ for BLGA. The horizontal dashed lines indicate the target average length at the end of the first cycle ($\bar{L}_{1,\mathrm{g}_1}$) and that at the end of the second cycle ($\bar{L}_{1,\mathrm{g}_2}$). The volume-weighted broadness of the measured PSSD along **(b)** the length and **(c)** the width direction, **(d)** the volume-weighted average aspect ratio, and **(e)** the volume-weighted broadness ratio before the experiment (s), at the end of the first cycle (g_1), and at the end of the second cycle (g_2, after the experiment). **(f)** Time t_{stage} required for the individual stages to reach their respective targets.

each stage (three stages per cycle) is visualized in Figure 6f. For the system BLGA in water, it is clear that the two growth stages are responsible for the largest part of the required process time. Still, the time required by the wet milling and the dissolution stages is significant as well. Note that two cycles (instead of just one cycle or more than two cycles) are chosen as a compromise between achieving a significant aspect ratio reduction and keeping the process time at reasonable values. In the doctoral thesis, a comparison between experiments comprising one and two cycles is presented along with experiments that are run to check the repeatability of the process outcome. These experiments indicate that the proposed control approach manages to reach the desired target repeatedly. Before applying the controlled multistage process to another needle-like compound, a few preliminary characterization steps need to be performed. These include, the characterization of the seed population, the identification of a constant supersaturation level at which growth occurs at a reasonable rate without any significant nucleation, and the evaluation of dissolution behavior to determine the heating rate applied in the dissolution controller. Two experiments are conducted with GDM. The first experiment is seeded with a batch of GDM seed crystals. In the second

experiment, the seeds are grown to a given target average length by means of a preliminary growth step at constant supersaturation followed by running the controlled multistage process. Based on running the experiments using GDM, it is observed that running the controlled multistage process for GDM is more challenging, because both its solubility and its growth and dissolution rates in the chosen solvent mixture are higher than those of BLGA in water. Still, it is shown that the controlled multistage process is able to achieve the process targets and to yield a significant shape change to more equant particles also in this case (see the doctoral thesis[1]). To conclude, an extension of a multistage process suggested previously[41,42] for the batch-wise transformation of needle-like seed crystals into more equant particles is presented with two unexplored striking features. First, the process is operated in a fully automated and controlled manner without the need of kinetic process models. Second, it provides robustness with respect to achieving PSSDs with desirable properties repeatedly over consecutive batches. Evidently, both of these developments are enabled by a combination of online monitoring of the particle size and shape evolution with feedback control techniques. It is worth acknowledging that future research would benefit from further improve-

ments in online size and shape monitoring and in processes with additional actuators for size and shape manipulation.

Relevance and Impact of the Thesis

The work presented in this thesis has led to improvements in characterizing the solid phase within the framework of a batch crystallization process. These improvements led to many interesting applications with a vast majority of them focussing on manipulating the size and shape of crystals exhibiting a needle-like morphology. Note that the work presented in this thesis is reflected in the seven publications in peer-reviewed journals.[2,12,14,21,27,29,40]

Imaging based techniques have proven to be powerful to provide reliable characterization of the solid phase. Nevertheless, there are always challenging issues at stake. The sheer number of crystals in a suspension, the wide variety of sizes and shapes exhibited by these crystals, the wide range of thermodynamic, kinetic, thermal and optical properties exhibited by these crystals, can barely scrap the surface with regard to the challenges. The motivation to tackle these problems has laid the initial foundation for a future work on characterizing and on manipulating the morphology of crystals that exhibit a platelet shape. Additionally, it must be noted that characterizing the solid phase in dense suspensions, close to industrial conditions, is critical. The design of a standalone dilution system coupled to the DISCO is currently undertaken by two graduate students. This suspension dilution setup is showing great promise in improving the operating range of the DISCO in terms of the suspension density by two orders of magnitude. Concerning the control of crystallization processes, the work presented in this thesis is serving as a guide to a doctoral thesis to develop better processes by addressing the pitfalls of the current work.

To conclude, the work presented in this thesis has been a culmination of years of research on monitoring, modeling and control of batch crystallization processes at ETH Zurich and elsewhere. It certainly appears that the research in the field of monitoring and control of crystallization will continue in the coming years. The various tools proposed in this thesis – has led to a small but significant advancements – for characterization and manipulation of size and shape of crystals. This will certainly aid both the academia and the industry to further improve the understanding and the robustness of crystallization processes.

Notes

The full doctoral thesis can be accessed at https://doi.org/10.3929/ethz-b-000369948

References

[1] Rajagopalan, A. K. A Dual Projection Imaging System to Characterize Crystallization Processes: Design and Applications. Doctoral Thesis, ETH Zurich, 2019.

[2] Rajagopalan, A. K.; Schneeberger, J.; Salvatori, F.; Bötschi, S.; Ochsenbein, D. R.; Oswald, M. R.; Pollefeys, M.; Mazzotti, M. *Powder Technol.* **2017**, *321*, 479–493.

[3] Davey, R.; Garside, J. *From Molecules to Crystallizers: An Introduction to Crystallization*; Oxford University Press: New York, NY, USA, 2000.

[4] Lovette, M. A.; Browning, A. R.; Griffin, D. W.; Sizemore, J. P.; Snyder, R. C.; Doherty, M. F. *Ind. Eng. Chem. Res.* **2008**, *47*, 9812–9833.

[5] Singh, M. R.; Chakraborty, J.; Nere, N.; Tung, H.-H.; Bordawekar, S.; Ramkrishna, D. *Cryst. Growth Des.* **2012**, *12*, 3735–3748.

[6] de Albuquerque, I.; Mazzotti, M.; Ochsenbein, D. R.; Morari, M. *AIChE J.* **2016**, *62*, 2974–2985.

[7] Bujak, B.; Bottlinger, M. *Part. Part. Syst. Charact.* **2008**, *25*, 293–297.

[8] Wang, X.; De Anda, J. C.; Roberts, K. *Chem. Eng. Res. Des.* **2007**, *85*, 921–927.

[9] Kempkes, M.; Vetter, T.; Mazzotti, M. *Chem. Eng. Sci.* **2010**, *65*, 1362–1373.

[10] Schorsch, S.; Vetter, T.; Mazzotti, M. *Chem. Eng. Sci.* **2012**, *77*, 130–142.

[11] Schorsch, S.; Ochsenbein, D. R.; Vetter, T.; Morari, M.; Mazzotti, M. *Chem. Eng. Sci.* **2014**, *105*, 155–168.

[12] Bötschi, S.; Rajagopalan, A. K.; Morari, M.; Mazzotti, M. *Cryst. Growth Des.* **2019**, *19*, 4029–4043.

[13] Bötschi, S. Optimization and Feedback Control of the Size and Shape Evolution of Elongated Crystals in Suspension. Doctoral Thesis, ETH Zurich, 2019.

[14] Bötschi, S.; Rajagopalan, A. K.; Morari, M.; Mazzotti, M. *J. Phys. Chem. Lett.* **2018**, *9*, 4210–4214.

[15] Simone, E.; Zhang, W.; Nagy, Z. K. *Cryst. Growth Des.* **2015**, *15*, 2908–2919.

[16] Hu, Y.; Liang, J. K.; Myerson, A. S.; Taylor, L. S. *Ind. Eng. Chem. Res.* **2005**, *44*, 1233–1240.

[17] Yang, Y.; Zhang, C.; Pal, K.; Koswara, A.; Quon, J.; McKeown, R.; Goss, C.; Nagy, Z. K. *Cryst. Growth Des.* **2016**, *16*, 7074–7082.

[18] Laurentini, A. *IEEE Trans. Pattern Anal. Mach. Intell.* **1994**, *16*, 150–162.

[19] Schöll, J.; Bonalumi, D.; Vicum, L.; Mazzotti, M.; Müller, M. *Cryst. Growth Des.* **2006**, *6*, 881–891.

[20] de Albuquerque, I.; Mazzotti, M. *Cryst. Growth Des.* **2014**, *14*, 5617–5625.

[21] Rajagopalan, A. K.; Bötschi, S.; Morari, M.; Mazzotti, M. *Cryst. Growth Des.* **2018**, *18*, 6185–6196.

[22] Braatz, R. D. *Annu. Rev. Contr.* **2002**, *26*, 87–99.

[23] Nagy, Z. K.; Braatz, R. D. *Annu. Rev. Chem. Biomol. Eng.* **2012**, *3*, 55–75.

[24] Nagy, Z. K.; Fevotte, G.; Kramer, H.; Simon, L. L. *Chem. Eng. Res. Des.* **2013**, *91*, 1903–1922.

[25] Patience, D. B.; Rawlings, J. B. *AIChE J.* **2001**, *47*, 2125–2130.

[26] Eisenschmidt, H.; Bajcinca, N.; Sundmacher, K. *Cryst. Growth Des.* **2016**, *16*, 3297–3306.

[27] Bötschi, S.; Rajagopalan, A. K.; Morari, M.; Mazzotti, M. *Cryst. Growth Des.* **2018**, *18*, 4470–4483.

[28] Bajcinca, N. *Comput. Chem. Eng.* **2013**, *58*, 381–389.

[29] Rajagopalan, A. K.; Bötschi, S.; Morari, M.; Mazzotti, M. *Cryst. Growth Des.* **2019**, *19*, 2845–2861.

[30] Seibert, K. D.; Collins, P. C.; Fisher, E. In *Chemical Engineering in the Pharmaceutical Industry: R&D to Manufacturing*; am Ende, D. J., Ed.; John Wiley & Sons, Ltd: Hoboken, NJ, USA, 2010; pp 365–378.

[31] Luciani, C. V.; Conder, E. W.; Seibert, K. D. *Org. Process Res. Dev.* **2015**, *19*, 582–589.

[32] Cote, A.; Sirota, E.; Moment, A. *Am. Pharm. Rev.* **2010**, *13*, 46–51.

[33] Harter, A.; Schenck, L.; Lee, I.; Cote, A. *Org. Process Res. Dev.* **2013**, *17*, 1335–1344.

[34] Engstrom, J.; Wang, C.; Lai, C.; Sweeney, J. *Int. J. Pharm.* **2013**, *456*, 261–268.

[35] Acevedo, D.; Kamaraju, V. K.; Glennon, B.; Nagy, Z. K. *Org. Process Res. Dev.* **2017**, *21*, 1069–1079.

[36] Yang, Y.; Pal, K.; Koswara, A.; Sun, Q.; Zhang, Y.; Quon, J.; McKeown, R.; Goss, C.; Nagy, Z. K. *Int. J. Pharm.* **2017**, *533*, 49–61.

[37] Salvatori, F.; Mazzotti, M. *Cryst. Growth Des.* **2018**, *18*, 5957–5972.

[38] Szilágyi, B.; Nagy, Z. K. *Cryst. Growth Des.* **2018**, *18*, 1415–1424.

[39] Ahmed, B.; Brown, C. J.; McGlone, T.; Bowering, D. L.; Sefcik, J.; Florence, A. J. *Int. J. Pharm.* **2019**, *554*, 201–211.

[40] Bötschi, S.; Rajagopalan, A. K.; Rombaut, I.; Morari, M.; Mazzotti, M. *Comput. Chem. Eng.* **2019**, *131*, 106581.

[41] Salvatori, F.; Mazzotti, M. *Ind. Eng. Chem. Res.* **2017**, *56*, 9188–9201.

[42] Salvatori, F.; Mazzotti, M. *Ind. Eng. Chem. Res.* **2018**, *57*, 15522–15533.

[43] Salvatori, F.; Binel, P.; Mazzotti, M. *Chem. Eng. Sci. X* **2019**, *1*, 100004.